



e-ISSN: 2319-8753 | p-ISSN: 2347-6710

IJRSET

International Journal of Innovative Research in
SCIENCE | ENGINEERING | TECHNOLOGY



INTERNATIONAL JOURNAL OF INNOVATIVE RESEARCH

IN SCIENCE | ENGINEERING | TECHNOLOGY

Volume 13, Issue 1, January 2024

ISSN INTERNATIONAL
STANDARD
SERIAL
NUMBER
INDIA

Impact Factor: 8.423

Design and Implementation of NN Based Solar PV and Grid Based Charging Station for Electric Vehicles

Dr. M. Vijaya Kumar M.Tech., Ph.D¹, P. A. Prabhakara M.Tech., (Ph.D)², S. Anusha M.Tech.,(Ph.D)³

M. Shirisha M.Tech⁴, K. Sasi Kiran Reddy⁵

RGUKT,(Vice-Chancellor i/c) & Professor & Rector in JNTUA College of Engineering (Autonomous), Ananthapuramu, Andhra Pradesh, India¹

Assistant Professor (Ad-hoc), JNTUA College of Engineering (Autonomous), Ananthapuramu, Andhra Pradesh, India²

Assistant Professor (Ad-hoc), JNTUA College of Engineering (Autonomous), Ananthapuramu, Andhra Pradesh, India³

Assistant Professor (Ad-hoc), JNTUA College of Engineering (Autonomous), Ananthapuramu, Andhra Pradesh, India⁴

PG-Scholar, JNTUA College of Engineering (Autonomous), Ananthapuramu, Andhra Pradesh, India⁵

ABSTRACT: This study proposes a multifunctional onboard converter equipped with an artificial neural network (ANN) controller to optimize the performance of electric vehicles (EVs). The converter seamlessly integrates solar photovoltaic (PV) and grid power sources, providing a versatile solution for EV energy management. The ANN controller intelligently manages power flow, enhancing the efficiency and adaptability of the onboard converter. Through the synergistic utilization of solar and grid power, the proposed system aims to contribute to the sustainable development of electric transportation while ensuring reliable and efficient energy utilization for EVs. The study explores the design, implementation, and performance evaluation of the proposed system, highlighting its potential impact on the broader landscape of electric vehicle technology.

KEYWORDS: Electric vehicles, on-board chargers, solar PV system, DC-DC converter, power factor correction.

I. INTRODUCTION

Usually, the electric vehicles (EVs) battery chargers are classified as off-board chargers and on-board chargers [1]. In off-board charging system, the charger is placed outside the vehicle premises at a charging station and provides a dc output which is directly plugged to the battery. This type of charger is not responsible for the vehicle weight; therefore, weight of these chargers is very high. As a result, it can be rated for high power and thus the EV battery can be charged within a few minutes. However, an impeding factor for the development of these chargers is the cost. Therefore, number of these chargers is limited and they are not ubiquitous. In on-board chargers, the battery can be directly charged from ac mains, which are widely available everywhere. This kind of charger does not require expensive infrastructure and vehicle can be charged anywhere, which is a clear advantage. They are further classified as conductive charging or inductive charging. In conductive charging system, the whole charging system is placed inside the vehicle. In inductive charging system, a part of the charger is placed outside of the vehicle [2]. The on-board chargers have to be light weight and small in size so that they can easily fit inside EVs. Further, the on-board chargers are more attractive for EVs because this types of charger is always available with vehicles. The on-board chargers are further classified as singlestage charger and two-stage charger. Moreover, in two-stage charger [3]–[5], a number of components are employed; therefore, two-stage charging solution is not much appealing for on-board implementation of charging system. While a single-stage charging system employs fewer number of components than two-stage charging system; therefore, it is more attractive for on-board application of EVs.

In conventional single-stage charging system, a bidirectional DC-DC converter is connected between DC-link of inverter and battery for power flow during PP and RB modes [6]. To eliminate this bidirectional DC-DC converter from single-stage charging system, power electronics researchers have proposed integrated type of chargers [6]–[10]. In the

integrated charger, the bidirectional DC-DC converter of conventional single-stage system connected between battery and DC-link is integrated with front-end converter at the cost of some additional switches. The overall integrated system has fewer number of total components compared to single-stage charging system. In the available literature integrated charging system utilizes non-isolated type of converters [11]. Moreover, magnetic isolation is desirable for vehicle application for safety of vehicle users as well as protection of charging circuit. Further reported integrated chargers use grid as main source for battery charging and alternatively battery is also charged with RB modes. The chargers [12]–[14] utilize only solar PV power source for battery charging and have the limitation of power indeterminacy; therefore, reliability of charger is sacrificed. However, recently a solar PV and grid based isolated 10-kW charger has been proposed in [15], which utilizes a large number of component as well as it does not operate in PP and RB modes. Based on the above literature review, this paper proposes a new grid and solar PV based single-stage integrated charging solution for on-board applications, as shown in Fig. 1.

The main features of the proposed PEC are summarized as (a) dual sources for charging operation, which enhances reliability of the charger, (b) galvanic isolation for better safety of vehicle users and charging circuit, (c) cost of conventional fuel sources based electricity per charge reduces, (d) achieves all modes of vehicle. Apart from above advantages of solar PV and grid based charging system, there are few additional advantages for battery charging with solar PV power, which are summarized as in Table I.

Converter topologies	Operation Modes				Number of components				Magnetic isolation
	PIC	solar PV charging	PP	RB	Switch	Diode	Inductor	Capacitor	
Integrated converter [7]	Buck-boost	NA	Buck-boost	Buck-boost	6	9	1	2	No
Integrated converter [8]	Boost	No	Boost	Buck	5	1	1	2	No
Integrated converter [9]	Boost	No	Buck-boost	Buck-boost	4	4	1	2	No
Integrated converter [10]	Buck-boost	No	Boost	Buck	3	4	2	3	No
Integrated converter [15]	Buck-boost	Buck-Boost	No	No	15	3	5	9	Yes
Proposed integrated converter	Buck-boost	Buck-boost	Boost	Buck	3	5	4	4	Yes

Table I Analysis of The Proposed Pec With Reported Methods

II. OPERATING MODES OF THE CONVERTER

In this section, operating modes of the proposed PEC are discussed in detail. States of the switching devices are shown in Table II.

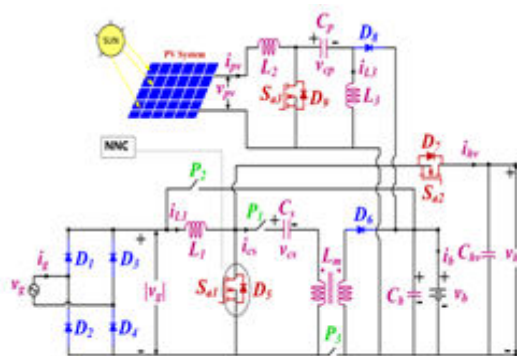


Fig .1 Configuration of the Proposed

A. Grid Mode

When solar power is not available, the battery is charged through grid power. When switch Sa1 turns ON, the rectified grid voltage is applied to inductor L1 and current through it builds up and L1 stores magnetic energy. The path of current through inductor L1 is shown by solid lines in Fig. 2. Moreover, the capacitor Cs transfers its stored energy to magnetizing inductor Lm of high frequency transformer (HFT). In this duration

Switching States of Semiconductor Devices and Mechanical Switches in All Modes

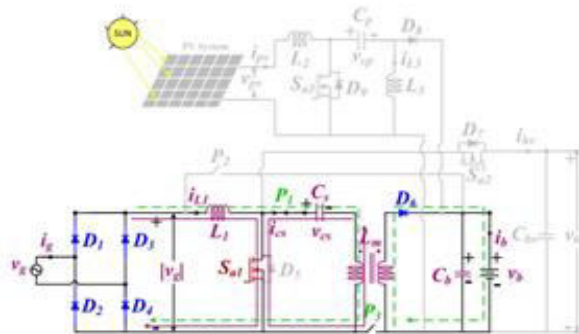


Fig. 2 Operation of the Proposed PEC during PIC mode

Operation mode	Figure	S_{a1}	S_{a2}	S_{a3}	P_1	P_2	P_3	D_5	D_6	D_7	D_8	D_9
PIC mode	Fig. 2	PWM	OFF	OFF	ON	OFF	OFF	OFF	ON	OFF	OFF	OFF
Solar PV mode	Fig. 3	OFF	OFF	PWM	ON	OFF	OFF	OFF	OFF	OFF	ON	OFF
solar PV and grid mode	Fig. 4	PWM	OFF	PWM	ON	OFF	ON	OFF	ON	OFF	ON	OFF
PP mode	Fig. 5(a)	OFF	PWM	OFF	OFF	ON	ON	OFF	OFF	ON	OFF	OFF
RB mode	Fig. 5(b)	OFF	OFF	PWM	OFF	ON	ON	ON	OFF	OFF	OFF	OFF

Table II Switching States of Semiconductor Devices and Mechanical Switches in All Modes

The battery is disconnected from the grid hence, capacitor C_b supplies power to the battery. When S_{a1} turns OFF stored energy of L_m is transferred to the battery through diode D_6 as shown by green dashed line and shown in Fig. 2.

B. Solar PV Mode

If grid power is not available, the battery is charged through only solar PV system and it is connected to the battery through SEPIC converter. The perturbed and observed based maximum power point Tracking (MPPT) controller is implemented through this SEPIC converter to optimize the performance of PV array. The equivalent circuit representation of this mode is shown in Fig. 3. When switch S_{a3} is turned-ON, current through inductors L_2 and L_3 flow as path indicated by pink and blue solid lines. When S_{a3} is turned-OFF, inductor L_3 imparts its stored energy to the battery through the diode D_8 . While inductor L_3 charges the capacitor C_p .

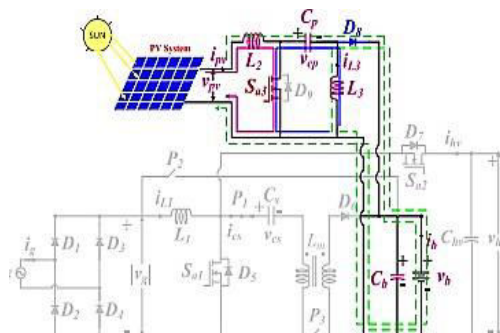


Fig.3 Operation of the Proposed PEC during solar PV mode

C.Solar PV and Grid Modes

This mode occurs when solar PV system is not able to generate required power (reference charging power) to charge the battery. In such condition, grid is supplying remaining power (reference power – solar PV power). The grid

and solar PV system both simultaneously charge the battery. If reference charging power is not met by solar PV system the rest of the power is supplied by the grid. The switch S_{a3} is operated through PWM to achieve MPPT operation and supplying power to the battery. The switch S_{a1} is operated for supplying power from grid to the battery. The equivalent circuit of this mode is shown in Fig. 4. PIC and solar PV modes (simultaneously).

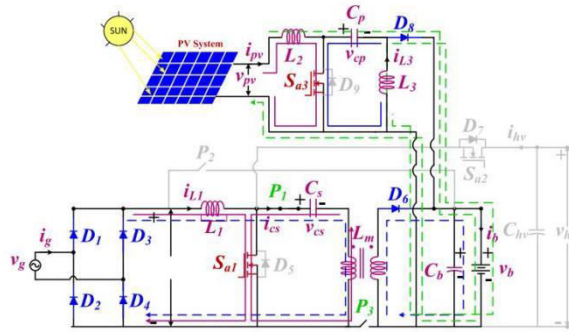


Fig. 4. Operation of the proposed PEC during PIC and solar PV modes (simultaneously).

D. PP Mode

The proposed system in this mode is operated as a conventional boost converter. The switch S_{a2} is operated through PWM signal, and mechanical switches P2 and P3 ON permanently ON. When S_{a2} is turned-ON voltage V_b is applied to inductor L1 and it stores magnetic energy and current flows through the path indicated in Fig. 5(a) by solid pink line. When S_{a2} is turned- OFF, inductor L1 is supplied its stored energy to the DC-link capacitor C_{hv} . The current path through various circuit elements has been shown with dotted lines in Fig. 5(a). The DC-link capacitor transfers its stored electrostatic energy to the load (motor drive system though an inverter). The vehicle will be in running mode as long as the battery is supplying energy to the DC-link capacitor.

E. RB Mode

The proposed system in this mode is operated as a conventional buck converter. The switch S_{a3} is operated through PWM signal, and mechanical switches P2 and P3 is permanently ON similar to the PP mode. When switch S_{a3} is turned ON inductor L1 stores energy through the path indicated by pink solid line in Fig. 5(b). When S_{a3} is turned OFF, stored energy of L1 is supplied to the load through the path indicated by green dotted lines, which is shown in Fig. 5(b).

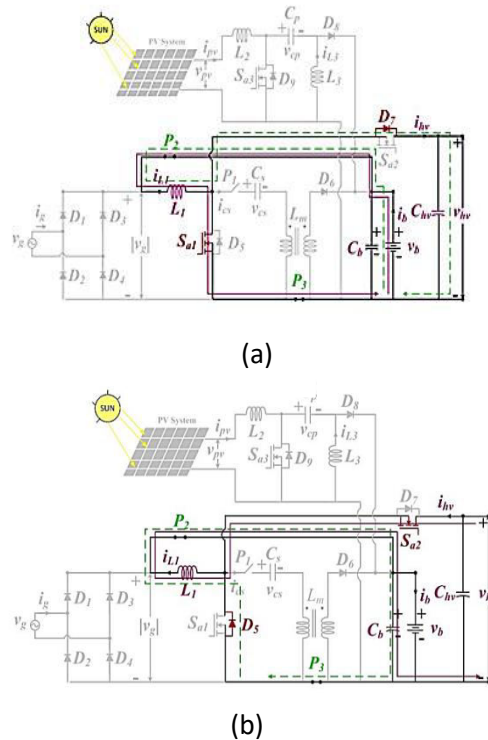


Fig. 5 Operation of the proposed PEC during in (a) PP mode, (b) RB mode

III. VOLTAGE AND CURRENT STRESS ANALYSIS

In this section, peak voltage and current stress analysis of the converter is investigated. Based on stress on the switching where NC = Not conducting, NIL = 0 V, $i_{L1,pp}$ = inductor L1 current in PP mode, $i_{L1,RB}$ = inductor L1 current in RB mode, $i_{Lm,grid}$ = magnetizing inductor Lm current in PIC mode, $i_{pv,max}$ = peak solar PV current devices, rating (voltage and current) of these devices is decided. In the proposed integrated system, some of the switching devices conduct for more than one mode. Therefore, their rating is selected based on the mode for which maximum voltage and current stress develop on the switching devices. Table III shows peak stress on the switching devices for all modes. The switch S_{a1} is utilized in PIC and PP modes. The voltage stress on S_{a1} in PIC mode is $(V_{g,max} + V_b)$ and in PP mode is V_b . Therefore, voltage rating of S_{a1} is selected based on PIC mode. The current rating of S_{a1} is also decided based on PIC mode because current stress on the switch S_{a1} is the sum of the input output current. The switch S_{a2} conducts only

Device	PIC		SPV		PP		RB	
	Voltage	Current	Voltage	Current	Voltage	Current	Voltage	Current
S_{a1}	$[V_{g,max} + V_b]$	$[i_{g,max} + (i_{Lm,grid})_{T_s} + \frac{\Delta i_{Lm,grid}}{2}]$	NIL	NC	V_b	$[(i_{L1,pp})_{T_s} + \frac{\Delta i_{L1,pp}}{2}]$	V_{hv}	NC
S_{a2}	N							$[(i_{L1,RB})_{T_s} + \frac{\Delta i_{L1,RB}}{2}]$
S_{a3}	N							NC
D_6	$[V_{g,max} + V_b]$	$[i_{g,max} + (i_{Lm,grid})_{T_s} + \frac{\Delta i_{Lm,grid}}{2}]$	V_b	NC	V_b	NC	V_b	NC
D_8	$[V_b]$	NC	$[V_{PV} + V_b]$	$[i_{pv,max} + (i_{LA,SPV})_{T_s} + \frac{\Delta i_{LA,SPV}}{2}]$	V_b	NC	V_b	NC
F_1	NIL	$i_{g,max} \max(1, \frac{V_{g,max}}{V_b})$	NIL	NC	V_b	NC	V_{hv}	NC
P_2	$[V_{g,max} - V_b]$	NC	NIL	NC	NIL	$[(i_{L1,pp})_{T_s} + \frac{\Delta i_{L1,pp}}{2}]$	NIL	$[(i_{L1,RB})_{T_s} + \frac{\Delta i_{L1,RB}}{2}]$
F_3	NIL	NC	NIL	NC	NIL	$[(i_{L1,pp})_{T_s} + \frac{\Delta i_{L1,pp}}{2}]$	NIL	$[(i_{L1,RB})_{T_s} + \frac{\Delta i_{L1,RB}}{2}]$

in RB mode. The peak voltage developed across switch S_{a2} in RB mode is V_{hv} . Therefore, the voltage rating of S_{a2} is selected as V_{hv} . The current rating of S_{a2} is decided based on only RB mode.

IV. DESIGN OF PASSIVE COMPONENTS

The design guideline of the passive components of the proposed PEC is an important step because some of the components is operated for more than one mode. Therefore, largest value among all modes is chosen as final value. The switching frequency is selected as 20 kHz for design of the passive components. Inductor L1 is operated in PIC, PP and

RB modes; therefore, its value is calculated for each mode. a) PIC Mode: The battery voltage v_b in PIC mode is given as [6].

$$V_b = \frac{d_1(t)}{(1 - d_1(t))} |v_g(t)| \quad (1)$$

where $d_1(t)$ is the duty ratio of the converter and expressed as:

$$d_1(t) = \frac{v_b}{v_b + |v_g(t)|} = \frac{v_b}{v_b + V_{g \max} |\sin(\omega t)|} \quad (2)$$

The value of L_1 for permitted current ripple (η) is given as [6], [17]

$$L_{1PIC} = \frac{v_g(t)d_1(t)}{\eta i_g(t) f_s} = \left(\frac{V_g^2}{P_g} \right) \frac{d(t)}{\eta f_s} = \frac{1}{\eta f_s} \left(\frac{V_g^2}{P_g} \right) \frac{V_b}{V_b + |V_g|} \quad (3)$$

The maximum ripple current in inductor is determined at the rated conditions i.e., $V_b = V_b \max$ and grid power $P_g = P_g \max$ for minimum value of grid voltage ($V_g \min$). The input inductor L_{1PIC} is designed for minimum peak grid voltage ($\sqrt{2} V_g \min$). Using (3), the calculated value of L_{1PIC} is 3.5 mH for permitted current ripple 10% of input current (i_g). b) PP Mode:

The value inductor L_1 in PP mode for allowable ripple current (η) is given as [6], [17], [18]

$$L_{1PP} = \frac{V_b d_2}{\eta' f_s} \quad (4)$$

where d_2 is equal to . For 10% of allowable ripple, the value of L_{1PP} is calculated as 1.65 mH. c) RB Mode: The value of L_1 in RB mode for allowable ripple current is given as [6], [17], [18]

$$L_{1RB} = \frac{V_b(1 - d_3)}{\eta'' f_s} \quad (5)$$

where d_3 is equal to V_b / V_{hv} . For 10% ripple current, the value L_{1RB} is calculated as 1.63 mH. The final value of inductor L_1 is selected as

$$L_1 = \max(L_{1PIC}, L_{1PP}, L_{1RB}) = \max(1.78, 1.65, 1.63) \quad (6)$$

Therefore, the final of L_1 is 1.78 mH and selected value for simulation experimentation studies. The value of magnetizing inductance L_m for ripple $\xi\%$ of the grid (i_g) is expressed as [19]

$$L_m = V_b \frac{(1 - d_1(t))}{\Delta I_{Lm}(t) f_s} = \frac{V_g^2}{P_g} \frac{1}{\xi f_s} \frac{V_b}{v_g(t) + V_b} \quad (7)$$

where $\Delta I_{Lm}(t) = \xi\%$ of the grid current (i_g). The turn ratio of HFT is selected as unity for this design. The value of L_m for a permitted current ripple (10% grid current) is calculated as 2.1mH and selected as 2mH for simulation and experimentation studies. The value of middle capacitor C_s for voltage ripple $k\%$ of V_{cs} is given as [6]

$$C_s = \frac{V_b d_1(t)}{k v_{cs}(t) f_s R_L} \quad (8)$$

where V_{cs} is the voltage across capacitor C_s by substituting $d1(t)$, $v_{cs}(t) = |v_g(t)|$ and equivalent load resistance $R_L = \frac{V_b}{2b/P_b}$ in (8), we can get

$$C_s = \frac{V_b}{k|v_g(t)|f_s \frac{V_b^2}{P_b}} \left(\frac{V_b}{|v_g(t)| + V_b} \right) = \frac{P_b}{k f_s (|v_g(t)| (|v_g(t)| + V_b))} \quad (9)$$

The value of capacitor C_s is estimated at peak magnitude of grid voltage ($V_g \text{ max}$) and at nominal battery voltage (V_b). Now, allowable ripple voltage is 5% of V_{cs} , the capacitance value of C_s after assuming 5% voltage across it is 0.823 μF and chosen as 1 μF . The capacitor C_b is chosen based on second harmonic (100 Hz) voltage ripple experienced by it. Therefore, size of capacitor is computed as [6]

$$C_b = \frac{I_b}{2\omega \Delta V_b} = \frac{\frac{P_b}{V_b}}{2\omega \delta V_b} = \frac{P_b}{2\omega \delta V_b^2} \quad (10)$$

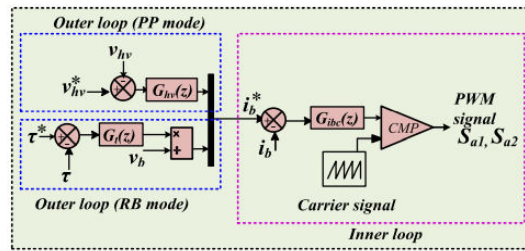
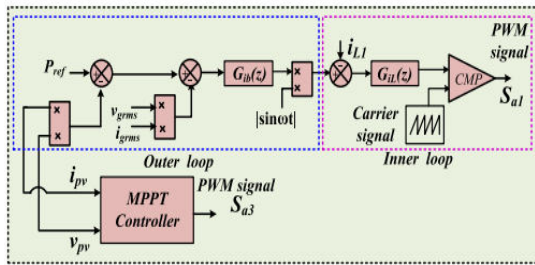


Fig. 6. Control strategy for PIC and solar PV modes. Fig. 7. Control strategy for PP and RB modes.

where δ represents the voltage ripple in (%) across capacitor C_b , $\omega = 2\pi fL$ and fL is the grid frequency (50 Hz). For 5% voltage ripple in C_b , the size of capacitor C_b using (10) is chosen as 1200 μF for simulation and experimentation studies. The DC-link capacitor C_{hv} is determined by PP mode, which is given as [18]

$$C_{hv} = \frac{d_2}{R f_s \frac{\Delta v_{hv}}{V_{hv}}} \quad (11)$$

where Δv_{hv} is the ripple voltage in capacitor C_{hv} . From (11), the value of C_{hv} is calculated as 83.5 μF for $\Delta v_{hv} = 1\%$ of V_{hv} . The selected value of C_{hv} is 100 μF . The design of MPPT converter (non-isolated SEPIC) is carried out in similar way as isolated SEPIC.

V. CONTROL ALGORITHM

In this section, control techniques for each mode of vehicle operation are discussed using Figs. 6 and 7. A. Control Technique for PIC and Solar PV Modes In PIC mode (alone), the battery is charged through the reference power P_{ref} . It is a two loop control strategy, the outer proportional integral (PI) regulator (or controller) $G_b(z)$ is supplied by error signal between set charging power and measured rectified grid side power. The outer PI regulator provides a reference DC signal, which is applied to the inner PI regulator $G_L(z)$. The signal generated from inner regulator is compared with high frequency saw tooth carrier signal to produce pulse width modulation (PWM) pulses for switch S_{a1} , as represented in Fig. 6. The PV array provides variable power to the battery bank depending upon availability of solar irradiance. A non-isolated SEPIC converter is used as a DC-DC interference between PV panel and battery storage

system. This converter has mainly two important functions, first is to optimize the performance of PV array and second to perform the buck and boost operation depending upon the environmental situation. A simple perturb and observe (P&O) based MPPT algorithm Is associated with the solar system is used because it is easy to implement for experimental study.

VI. RESULTS AND DISCUSSION

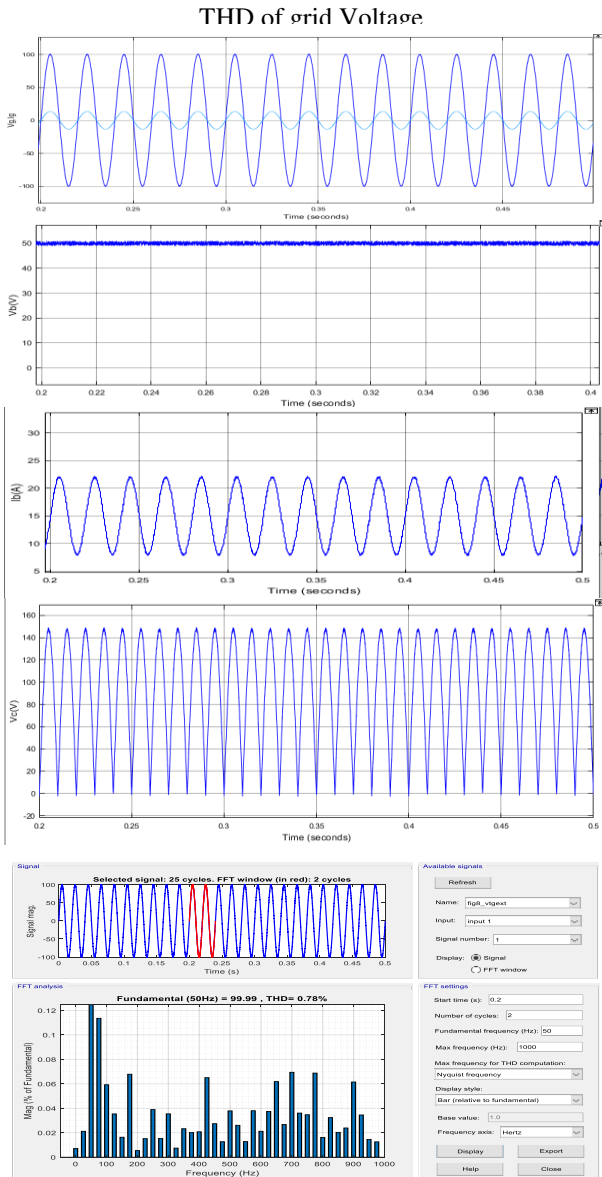


Fig.8 Simulation waveforms of PIC mode (alone) a)grid voltage and grid current, b)voltage across capacitor

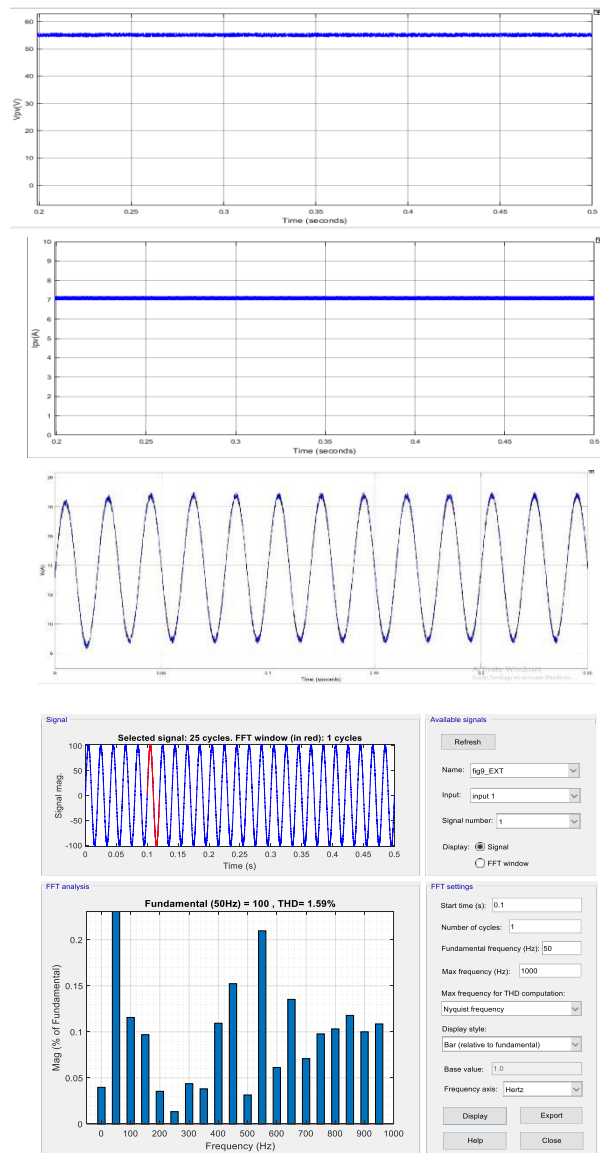


Fig.9 simulation waveforms of Solar PV modes a)solar PV current, b)solar PV voltage, c) Battery current d)THD

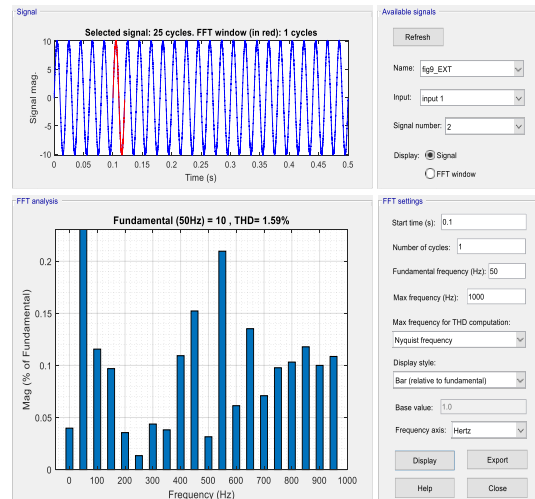
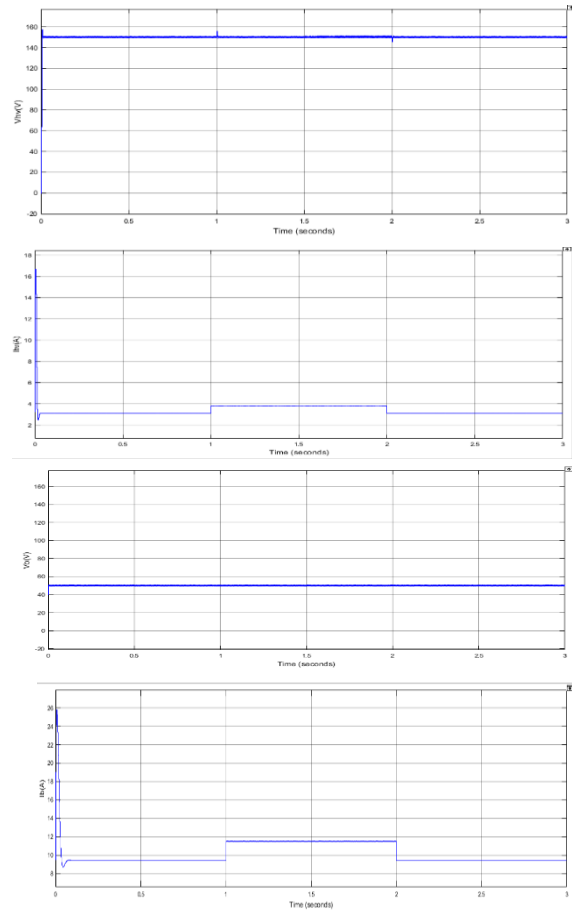
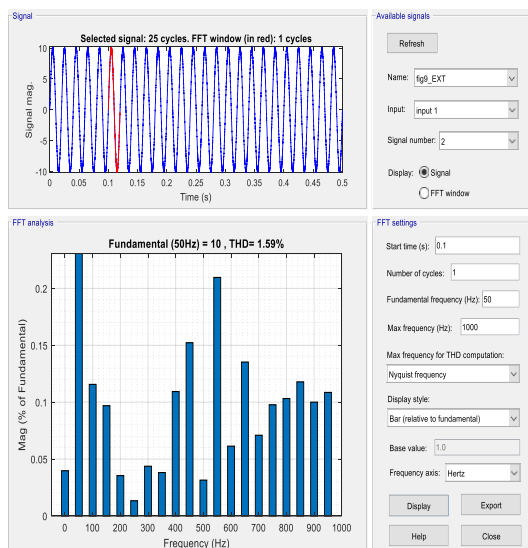
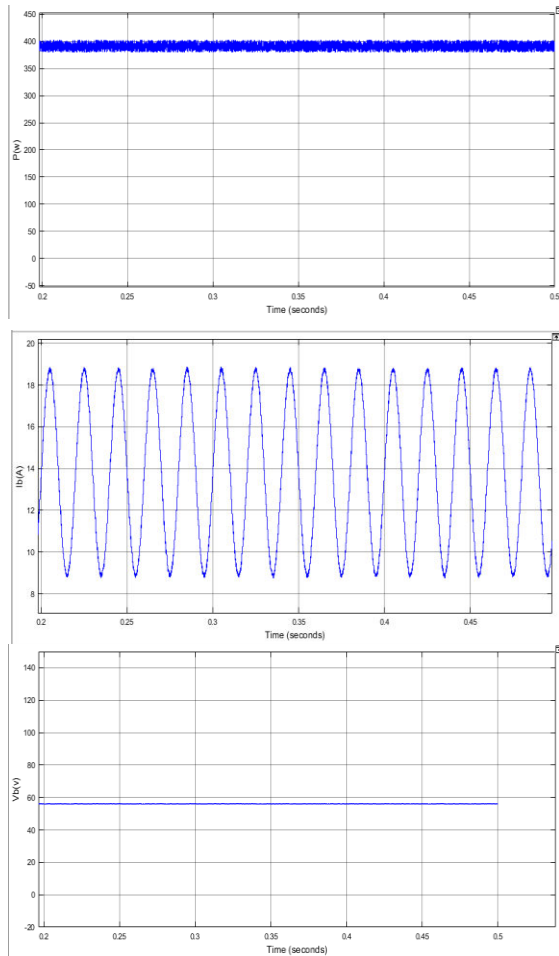


Fig 10. simulation waveforms of PIC and solar PV modes (simultaneously) grid voltage and grid current, solar PV voltage, solar PV current, solar PV power , battery voltage,

Fig. 11. Simulated waveforms of PP mode (a) DC-link voltage, (b) DC-link current, (c) battery voltage, (d) battery current

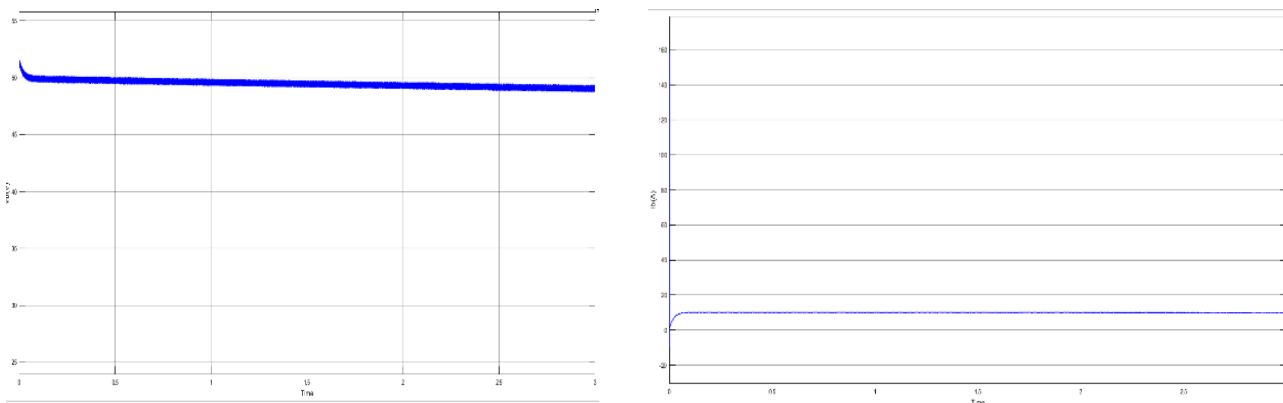


Fig. Simulated waveforms of RB mode (a) DC-link voltage, (b) battery voltage, (c) battery current

VII. CONCLUSION

In this work, a new power electronic converter (PEC) has been developed for plug-in electric vehicles (PEVs) utilizing both grid and solar PV sources. The proposed PEC has capability to operate for all modes of vehicles, i.e., charging, propulsion (PP) and regenerative braking (RB). The charging is achieved through grid (plug-in charging (PIC)) and solar PV system. The proposed PEC is operated as an isolated SEPIC during charging from grid and as a non-isolated SEPIC during solar PV charging. While, in PP and RB modes, it operates as a conventional boost and buck converters, respectively. Conventional boost and buck operation of the converters provide low stresses on switching devices than SEPIC operation of the converter. Therefore, stress on switching devices in PP and RB modes are lower than PIC and solar PV modes, which is desirable for vehicle application because usually PP and RB modes rated for high power than PIC and solar PV modes. The modes of the proposed system have been validated through computer simulation and prototype model for 800 W charging power and 48 V battery. The overall system provides a reliable and efficient solution for electric vehicle battery charging system and can be a promising solution for future electric vehicles.

REFERENCES

- [1] M. Yilmaz and P. T. Krein, "Review of battery charger topologies, charging power levels, and infrastructure for plug-in electric and hybrid vehicles," *IEEE Trans. Power Electron.*, vol. 28, no. 5, pp. 2151–2169, May 2013.
- [2] T. W. Ching and Y. S. Wong, "Review of wireless charging technologies for electric vehicles," in *Proc. 5th Int. Conf. Power Electron. Syst. Appl.*, Dec. 2013, pp. 1–4.
- [3] O. C. Onar, J. Kobayashi, D. C. Erb, and A. Khaligh, "A bidirectional high-power-quality grid interface with a novel bidirectional noninverted buck-boost converter for PHEVs," *IEEE Trans. Veh. Technol.*, vol. 61, no. 5, pp. 2018–2032, Jun. 2012.
- [4] J. C. Bendien, G. Fregien, and J. D. van Wyk, "High-efficiency on-board battery charger with transformer isolation, sinusoidal input current and maximum power factor," *IEE Proc. B - Electric Power Appl.*, vol. 133, no. 4, pp. 197–204, Jul. 1986.
- [5] A. V. J. S. Praneeth and S. S. Williamson, "A wide input and output voltage range battery charger using buck-boost power factor correction converter," in *Proc. IEEE Appl. Power Electron. Conf. Expo.*, Mar. 2019, pp. 2974–2979.
- [6] A. K. Singh and M. K. Pathak, "Integrated converter for plug-in electric vehicles with reduced sensor requirement," *IET Elect. Syst. Transp.*, vol. 9, no. 2, pp. 75–85, 2019.
- [7] Y. J. Lee, A. Khaligh, and A. Emadi, "Advanced integrated bidirectional AC/DC and DC/DC converter for plug-in hybrid electric vehicles," *IEEE Trans. Veh. Technol.*, vol. 58, no. 8, pp. 3970–3980, Oct. 2009.
- [8] S. Dusmez and A. Khaligh, "A charge-nonlinear-carrier-controlled reduced-part single-stage integrated power electronics interface for auto motive applications," *IEEE Trans. Veh. Technol.*, vol. 63, no. 3, pp. 1091–1103, Mar. 2014.
- [9] S. Dusmez and A. Khaligh, "A compact and integrated multifunctional power electronic interface for plug-in electric vehicles," *IEEE Trans. Power Electron.*, vol. 28, no. 12, pp. 5690–5701, Dec. 2013.

- [10] A. K. Singh and M. K. Pathak, "A multi-functional single-stage power electronic interface for plug-in electric vehicles application," *Electric Power Compon. Syst.*, vol. 46, no. 2, pp. 135–148, 2018.
- [11] D. Patil, M. Sinha, and V. Agarwal, "A cuk converter based bridgeless topology for high power factor fast battery charger for electric vehicle application," in *Proc. IEEE Transp. Electrification Conf. Expo.*, Jun. 2012, pp. 1–6.
- [12] S. Biswas, L. Huang, V. Vaidya, K. Ravichandran, N. Mohan, and S. V. Dhople, "Universal current-mode control schemes to charge Li-ion batteries under DC/PV source," *IEEE Trans. Circuits Syst. I: Reg. Papers*, vol. 63, no. 9, pp. 1531–1542, Sep. 2016.
- [13] J. Traube et al., "Mitigation of solar irradiance intermittency in photovoltaic power systems with integrated electric-vehicle charging functionality," *IEEE Trans. Power Electron.*, vol. 28, no. 6, pp. 3058–3067, Jun. 2013.
- [14] D. Venkatramanan and V. John, "Dynamic modeling and analysis of buck converter based solar PV charge controller for improved mppt performance," in *Proc. IEEE Int. Conf. Power Electron., Drives Energy Syst.*, Dec. 2018, pp. 1–6.
- [15] G. R. C. Mouli, J. Schijffelen, M. van den Heuvel, M. Kardolus, and P. Bauer, "A 10 kw solar-powered bidirectional EV charger compatible with chademo and combo," *IEEE Trans. Power Electron.*, vol. 34, no. 2, pp. 1082–1098, Feb. 2019.
- [16] G. R. C. Mouli, P. Bauer, T. Wijekoon, A. Panosyan, and E. Barthlein, "Design of a power-electronic-assisted OLTC for grid voltage regulation," *IEEE Trans. Power Del.*, vol. 30, no. 3, pp. 1086–1095, Jun. 2015.
- [17] T. M. U. N. Mohan and W. P. Robbins, *Power Electronics: Converters, Applications and Design*. Hoboken, NJ, USA: Wiley, 2009.
- [18] D. Hart, *Power Electronics*. New York, NY, USA: McGraw-Hill, 2011.
- [19] V. Bist and B. Singh, "A unity power factor bridgeless isolated CUK converter-fed brushless dc motor drive," *IEEE Trans. Ind. Electron.*, vol. 62, no. 7, pp. 4118–4129, Jul. 2015. [20] M. S. Ngan and C. W. Tan, "A study of maximum power point tracking algorithms for stand-alone photovoltaic systems," in *Proc. IEEE Appl. Power Electron. Colloquium*, Apr. 2011, pp. 22–27.
- [21] A. S. Ahmed, B. A. Abdullah, and W. G. A. Abdelaal, "MPPT algorithms: Performance and evaluation," in *Proc. 11th Int. Conf. Comput. Eng. Syst.*, Dec. 2016, pp. 461–467.
- [22] S. Deo, C. Jain, and B. Singh, "A PLL-less scheme for single-phase grid interfaced load compensating solar PV generation system," *IEEE Trans. Ind. Informat.*, vol. 11, no. 3, pp. 692–699, Jun. 2015. [23] A. K. Mishra and B. Singh, "Control of SRM drive for photovoltaic powered water pumping system," *IET Electric Power Appl.*, vol. 11, no. 6, pp. 1055–1066, 2017.



INTERNATIONAL
STANDARD
SERIAL
NUMBER
INDIA



INTERNATIONAL JOURNAL OF INNOVATIVE RESEARCH

IN SCIENCE | ENGINEERING | TECHNOLOGY

 9940 572 462  6381 907 438  ijirset@gmail.com



www.ijirset.com

Scan to save the contact details